Parker, A., Jennings, R., Parton, A., Clark-Balzan, L., White, T., Groucutt, H., Breeze, P., Drake, N. and Petraglia, M. (2016) 'Human occupation of the northern Arabian interior during early Marine Isotope Stage 3', *Journal of Quaternary Science*, 31 (8)

DOI: https://doi.org/10.1002/jqs.2920

Human occupation of the northern Arabian interior during early Marine Isotope Stage 3

Richard P. Jennings[1], Ash Parton[2,3], Laine Clark-Balzan [4] Tom S. White[2], Huw S. Groucutt[2], Paul Breeze[5], Adrian Parker[3], Nick A. Drake[5], Michael D. Petraglia[6]

[1] School of Natural Sciences and Psychology, Liverpool John Moores University, James Parsons Building, Byrom St, Liverpool L3 3AF, United Kingdom.

[2] School of Archaeology, Research Laboratory for Archaeology and the History of Art, University of Oxford, Hayes House, 75 George St, Oxford, OX1 2PG, United Kingdom.

[3] Department of Social Sciences, Oxford Brookes University, Gibbs Building, Gipsy Lane, Oxford, OX3 0BP United Kingdom

[4] Albert-Ludwigs-Universitat Freiburg, Freiburg im Breisgau, Baden-Württemberg, DE

[5] Department of Geography, King's College London, K4U.06 Strand Campus, London WC2R 2LS, United Kingdom.

[6] Max Planck Institute for the Science of Human History, Kahlaische Strasse 10, D-07743, Jena, Germany

[1]Corresponding author: Richard Jennings. Email: R.P.Jennings@ljmu.ac.uk
Tel: +44 (0) 0151 904 6301

Abstract

The early part of Marine Isotope Stage (MIS) 3 (c. 60– 50 ka) is a crucial period for studying human demography and behaviour in Southwest Asia, and how these relate to climatic changes. However, the archaeological and palaeoenvironmental records for MIS 3 in critical areas such as the Arabian Peninsula remain poorly developed. Here, we present findings from the Al Marrat basin in the Nefud desert, which provides the first clear evidence for both increased humidity and human occupation of the interior of northern Arabia during early MIS 3. A Middle Palaeolithic assemblage, dated by OSL to c. 55 ka, was found stratified within a sequence of relict palustrine deposits indicative of shallow water body formation in the Al Marrat basin. Hominin presence in northern Arabia at this time coincides with the intensification and northward displacement of monsoon rainfall systems during a period of maximum insolation. These findings add to a growing corpus of palaeoenvironmental evidence, which indicates that the Arabian interior was neither arid nor unpopulated during early MIS 3, and that hydrodynamic responses to enhanced moisture availability facilitated demographic expansions into the Arabian interior.

Keywords: MIS 3, Middle Palaeolithic, Levallois, Arabia, OSL,

palaeoenvironmental reconstruction

1. Introduction

Early Marine Isotope Stage 3 (MIS) 3 (60–50 ka) is a critical period in the study of human evolution in Southwest Asia, with palaeontological and archaeological data indicating that Neanderthals (and possibly *Homo sapiens*) were present in the Levant in this period (e.g. Akazawa *et al.*, 1998; Shea

2003; Hershkovitz *et al.*, 2015). Recent genetic studies have indicated that the Middle East may have been a nexus of admixture between these species (Green *et al.*, 2010, Fu *et al.*, 2014). The Upper Palaeolithic began here at c. 50-45 ka, although Middle Palaeolithic technologies remained prevalent. Little is known, however, about population dynamics in the Arabian Peninsula at this time. Some dispersal models have sidelined the Arabian interior during MIS 3, preferring to focus on hypothesized coastal routes out of Africa (e.g. Mellars *et al.*, 2013; Eriksson *et al.*, 2012). An important aspect of such coastal dispersal models is the view that inland Arabia remained arid and incapable of supporting populations at this time (e.g. Fleitmann *et al.*, 2011; Rosenberg *et al.*, 2011). In addition, archaeological evidence for occupation of the interior during MIS 3 is extremely sparse, with just two dated sites reported not deep in the interior but relatively near coastlines: Shi'bat Dihya-1 (SD-1) in western Yemen (c. 55 ka; Delagnes *et al.*, 2012) and Assemblage A at Jebel Faya, UAE (c. 40 ka; Armitage *et al.*, 2011).

There is, however, increasing climatic evidence for a pluvial episode during early MIS 3. Although this pluvial was not as prolonged or intense as previous humid phases such as those of MIS 5, the period in which human populations are thought to have first expanded into the region (Petraglia *et al.,* 2012; Groucutt *et al.,* 2015a, Groucutt *et al.,* 2015b, Groucutt *et al.,* 2015c; Parton *et al.,* 2015; Jennings *et al.,* 2015), the hydrological effects would still have been wide ranging. In Oman and the UAE, the activation of drainage systems is recorded at c. 55 ka, following the development of alluvial fan processes along the western Hajar Mountains (Krbetschek, 2008; Blechschmidt *et al.*, 2009; Farrant *et al.*, 2012; Parton *et al.*, 2013; 2015; Hoffmann *et al.*, 2015). Drainage activation is also indicated by the deposition of gravels dated to c. 54 ka in the centre of the Arabian peninsula (McLaren *et al.*, 2008), while an age of 67 ± 9 ka from sands underlying lacustrine carbonates is also reported

from the southern Rub' al-Khali (Matter *et al.*, 2015). The increase in rainfall indicated in these records is supported by speleothems from Socotra, which record an abrupt intensification and northward displacement of monsoon rainfall during early MIS 3 (Burns *et al.*, 2003). To the north, mid-late MIS 3 lake deposits have been recorded in Jordan (e.g. Schuldenrein and Clark, 1994; Moumani *et al.*, 2003; Cordova *et al.*, 2013), while speleothem growth has been dated to ~ 61 ka in the northern Negev (Vaks *et al.*, 2006). The relevance of these Mediterranean moisture sources to more southerly regions is debated, however, due to a lack of speleothem growth in the central and southern Negev. This suggests that the southward transport of Mediterranean moisture during early MIS 3 was limited to the northern Negev (Vaks *et al.*, 2010), and that regions such as the Levant may have received more regular rainfall compared to the monsoon-influenced areas to the South (e.g. Jennings *et al.*, 2015).

Although the spatio-temporal variability of rainfall across Arabia during early MIS 3 remains unresolved, it is becoming clear that both northern and southern regions of the Arabian Peninsula experienced some degree of increased humidity during this period. In light of this, we present findings from Al Marrat 3, the first stratified Middle Palaeolithic site recorded in the interior of the Arabian Peninsula dated to early MIS 3 (Figure 1).

2. Environmental Setting

The site of Al Marrat 3 (ALM 3) is located within the Al Marrat basin at the southern margin of the Nefud Sand Sea in Ha'il Province, Saudi Arabia (Figure 1). The basin is situated at ~ 850 m above sea level and is one of nine depressions that occur on the leeward side of outcrops of Palaeozoic sandstone bedrock (jebels). The presence of the jebels has served to shelter the basin from eastward transport and deposition of aeolian sand, resulting in a topographic depression approximately 9 x 2.5 km. The basin is situated 50 km south of the Jubbah Palaeolake, the most well-known of these depressions, which contains an extensive suite of palaeolake sediments and numerous archaeological sites dating to MIS 5 and the early Holocene

(Petraglia *et al.*, 2011; 2012; Crassard *et al.*, 2013; Groucutt *et al.*, 2015d; Hilbert *et al.*, 2014).

Figure 1 - Location map

3. Materials and methods

The archaeological potential of the Al Marrat basin was identified through remote sensing palaeolake detection techniques (Breeze *et al.*, 2015). Palaeolake deposits were detected in each of the nine observed basins, indicating that they had filled with water during previous humid periods (Breeze *et al.*, 2015).

A field survey of the basin was undertaken to record archaeological sites and investigate the nature of the large areas of detected palaeolake deposits, many of which were found to be preserved as inverted relief features (IRFs). These features are low relief mounds which have often been found to preserve palaeoenvironmental and archaeological evidence elsewhere in Arabia (Petraglia *et al.*, 2012; Hilbert *et al.*, 2014; Groucutt *et al.*, 2015c, Groucutt *et al.*, 2015d). During this survey, the IRF at Al Marrat 3, which measures 18 m x 14 m with a height of 1.3 m, was identified, excavated and sampled for various palaeoenvironmental analyses. A trench measuring 4 m x 1 m was excavated where Middle Palaeolithic artefacts were observed eroding from the slopes of the feature. Eight stratigraphic units were observed from the calcretized top of the mound to its base.

Samples were extracted from a stratified sequence of sands and palustrine carbonate deposits to a depth of 1.3 m for palaeoenvironmental analyses. Analyses of organic carbon (LOI_{org}) and carbonate content (LOI_{carb}) were conducted following the standard procedure described by Dean (1974) and Heiri *et al.* (2001), while environmental magnetic susceptibility measurements were determined following Dearing (1999). For laser granulometry of the <2 mm sediment component, samples were disaggregated in de-ionised water with 5% sodium hexametaphosphate, and analysed using a Malvern

Mastersizer 2000. Phytoliths were analysed where they were preserved. Samples for phytolith analysis were prepared using the methodology outlined in Parker *et al.* (2011). The lithic assemblage was analysed using the methods outlined in Scerri *et al.* (2015) and Groucutt *et al.* (2015c).

Two optically stimulated luminescence (OSL) tube samples were collected from the site; one from Unit 3 and one from Unit 4. Preparation and measurement of coarse grain quartz (180-255 μm) extracts were conducted at the University of Oxford (RLAHA) under subdued amber light (sodium lamps: 588 nm; LEDs: 590 nm). Samples were opened, and the light exposed ends were removed. A 10-15 g portion was retained for ICP-MS analysis. The interior sediment was wet sieved and carbonates were digested with 10% hydrochloric acid. The desired size fraction was then dried, and feldspars were removed via density separation with sodium polytungstate (ρ = 2.58 g cm^{-3}). Quartz was etched with hydrofluoric acid (60% for 90 minutes), treated again with hydrochloric acid to remove precipitated fluorites, and finally second sieved to eliminate grain fragments <180 μm in diameter. Both single grain and multigrain (18 aliquots, 3-4 mm diameter) equivalent doses (D_Es) were measured, using a single aliquot regeneration protocol (Table S1), which included recycled dose, zero dose, and IR depletion steps (Duller, 2003). A dose recovery experiment (6 multigrain aliquots, 3-4 mm) was also performed for sample ALM3-OSL3. Aliquots were bleached with blue LEDs (NSPB-500S, 470Δ20 nm) for 300 s at 25 ^{0} C and irradiated (136.6 ± 2.7 Gy). The given dose was recovered via the multigrain SAR protocol. Data was analysed via Luminescence Analyst v.4.11, and the final equivalent dose (D_E) for each sample was determined from accepted aliquots (Table 1) via the central age model (CAM: Galbraith *et al*., 1999). Dose rates (Table 2) were calculated as reported in Hilbert *et al.* (2014). The Th/U ratio of the sediments is significantly less than the expected value (3-4), due probably to the relatively high proportion of carbonate in this environment (Faure, 1986). Nevertheless, secular disequilibrium is expected to change the OSL ages by a proportion less than the estimated error (~ 7-10%) due to the use of the field gamma spectrometer and the age of the samples (Olley *et al.,* 1996, 1997).

Tables 1-2 - OSL dating

4. Results

4.1. Basin survey

Seven archaeological sites (ALM 1-7) from multiple periods were discovered during the survey. These indicate recurrent occupation of the basin (Table 3, Figure 2). ALM 6 and ALM 7 represent the earliest episodes of occupation and were identified as Acheulean. These comprised low-density distributions of bifaces and occasional cleavers located on IRFs at the western basin extent (Shipton *et al.*, 2014). Low-density Middle Palaeolithic scatters were identified in the northeast and central-SW of the basin (ALM 1 and ALM 5), atop the large areas of gypsiferous IRFs detected by the remote sensing method that led to the initial survey. Rock art panels and megalithic structures (ALM 2 and ALM 4) identified on the basin margins indicate the presence of Holocene populations within the region

Table 3 - Archaeological sites found in the Al Marrat basin

Figure 2 - Al Marrat basin and archaeological sites

The most significant discovery was made in the west-central area of the basin at Al Marrat 3. Here, Middle Palaeolithic artefacts were observed in a discrete location on one slope of an IRF (Figure 3). This IRF, being heavily indurated, had not been individually detected by the remote sensing due to its spectral signature being closer to that of the bedrock, in contrast with IRFs elsewhere in the basin.

Figure 3 - IRF plan view and trench location

4.2. Al Marrat 3 stratigraphic profile

The Al Marrat 3 sequence comprises seven interstratified marls and calcretes, reflecting climatically driven changes in the basin (Figure 4). The Pleistocene

deposits are underlain by sandstone bedrock, which has been partially dissolved as a result of water body formation in the basin. This dissolved material consists of poorly sorted fine quartz sands (Unit 1), which progress into very poorly sorted fine-medium iron-stained sands with vertical root voids throughout (Unit 2). This unit represents the onset of humidity in the region, marked by an influx of fluvial sediments and the initial development of vegetation. This is reflected through sharp increases in magnetic susceptibility and organic content values. These sediments are overlain by Unit 3, which comprises very poorly sorted, marly silts with high carbonate content values, representing the formation of a water body in the basin. Evidence of root activity throughout this unit likely indicates relatively shallow water conditions where vegetative processes could persist, or where periodic sub-aerial exposure affected the lacustrine system (e.g. a littoral setting). Phytoliths (Table 4) were almost exclusively absent towards the base of this unit with signs of corrosion and pitting on the few morphotypes observed suggesting either an absence of vegetation or most likely post-depositional silica dissolution. Towards the top of the unit phytolith preservation is also sparse but there is less sign of pitting and corrosion. Only grassland morphotypes were represented by round, square, oblong types with a few bulliform and elongate smooth forms present. Some bilobate and cross-body types present, which are typically from Panicoid grasses were also observed. A lack of laminations or evidence for increased redox (i.e. the stratification of iron oxide due to seasonal lake level variations), indicate a continuous phase of deposition for this unit, and that water levels did not fluctuate significantly.

Figure 4 – Al Marrat 3 Stratigraphic profile

Table 4 – Phytoliths from Al Marrat 3

Unit 4 marks a change in the regional climate around Al Marrat and a shift to drier conditions. A diffuse contact separates Unit 4 from Unit 3 suggesting a gradual rather than abrupt change in sedimentation. The unit is comprised of blocky, nodular calcareous platykurtic silts with numerous root voids and occasional gypsiferous nodules throughout. These sedimentological features

suggest an occasional desiccation and fragmentation of the exposed palustrine carbonates, possibly due to a lowering of water levels, or increased evaporation rates. Nonetheless, although indicative of a generally dry environment, climatic conditions at this time appear to have been more humid than today. Phytoliths were well preserved in Unit 4 but the counts were relatively low (n=176). Phytoliths were exclusively derived from grassland vegetation. Short-bodied grass cells dominate this part of the sequence (0.45 m) accounting for up to 80% of the total sum. These are mainly round, small square, oblong forms which are usually associated, but not exclusively, with Pooids. Lobate morphotypes derived from tall mesic C_4 Panicoid grass comprises 1.1 % of the total sum, while saddle morphotypes derived from C_4 arid-adapted Chloridoid grasses account for ~1.7 %. No circular rugose morphotypes were present indicating an absence of trees in the immediate landscape. Long cell morphotypes comprised 20% of the total sum with bulliforms (11.4%), points (4.6 %) and elongate smooth (3.4 %) also present.

Unit 5 comprises a transitional horizon of incipient calcrete formation, with an increased influx of coarser, mesokurtic sand material and decreasing organic content values. This likely represents increasingly arid conditions in the region with greater aeolian influx; further evidenced by the presence of larger gypcrete blocks and occasional calcrete nodules following the partial replacement of the host material within the vadose zone under more evaporitic conditions. Phytolith preservation was generally good in Unit 5 with a very similar pattern of vegetation shown to that described in Unit 4 at 0.45 m. The only difference is the very low occurrence of circular rugose forms (1.2 %) indicating the presence of woody vegetation derived from trees or shrubs. Also present were very low numbers of trapezoid forms characteristic of Cyperaceae (sand sedge).

The overlying units (Units 6 & 7) indicate continued environmental deterioration (increased aridity) in the region with the continued influx of coarser sand and formation of highly weathered calcrete nodules in a soft, friable sandy matrix. A highly indurated calcretized mantle is indicative of the final stage of drying in the basin, and caps the softer sediments beneath. This

likely formed as a subsurface calcic horizon following the leaching and rapid precipitation of carbonates during surface desiccation. Phytolith preservation in Unit 6 was poor with only 17 samples observed. Unit 7, however, had very good phytolith preservation characterised by short cells (85%) with long cells forming a much lower proportion (15). Round, square and oblong forms dominate the assemblage accounting for ~ 72 of the total sum. Lobates from Panicoids formed 1.5 %, while saddles from Chloridoids comprised 3.7%. A presence of some woody vegetation was suggested by a trace of circular rugose forms (1.2 %). Long cells were represented by elongate smooth (7.7%), points (5.9%) and bulliforms (1.2%).

4.3 Al Marrat 3 luminescence dating

Five of six multigrain aliquots measured during the dose recovery experiment were accepted for analysis, with one excluded due to its IR depletion ratio (probable feldspar contamination). The population of recovered D_Es from the accepted aliquots was not overdispersed (σ=0), and the recovered common age D_E was within one sigma uncertainty of the given dose (Table 2). Though individual aliquot estimates are more scattered, three of five also have individual D_Es within one sigma of the given D_E. Given the single grain results discussed below, we suggest that most aliquots are dominated by signals derived from fewer than five grains, and this is likely to explain the spread in data. Overall, the SAR protocol used here seems appropriate for these samples.

Figure 5 - OSL dating

The majority of multigrain aliquots measured for age determination passed all rejection criteria (Table 1, Figure 5). Two were rejected from each sample for unsuitable recycling ratios, but none showed significant recuperation. Overdispersion values of the accepted populations are slightly higher than for other multigrain aliquots measured for samples from similar sites in the Nefud desert: between 24 ± 3% and 29 ± 4% calculated for small aliquots (~ 50 grains) from a calcrete and palaeosols (Petraglia *et al.*, 2011), and between

12 and 28% for a suite of primarily aeolian quartz multigrain samples of unknown size (Rosenberg *et al.*, 2013). Only one aliquot (sample ALM3-OSL3) is saturated.

Single grains were primarily rejected due to low natural test dose signal intensity or high error (81% of grains from both samples, Table 1). Of those passing these criteria, a further fifth to a quarter of grains were excluded for unsuitable recycling ratios, with smaller proportions excluded due to recuperation or IR response. 1.7% and 3% of grains from samples ALM3-OSL2 and ALM3-OSL3, respectively, were accepted according to these criteria. Saturated grains were noted for both samples, and a maximum of 15% of accepted grains (ALM3-OSL3) were excluded due to saturation. These single grain characteristics are similar to those reported by multiple studies for quartz from the Arabian peninsula, with 86-92% of grains rejected due to low signal intensity and 1-4% accepted for age calculation (Armitage *et al*., 2011; Petraglia *et al.*, 2012; Groucutt *et al.*, 2015c). Overdispersion values measured for single grain populations (30.7 ± 5.6% and 45.7 ± 8.1%) are also typical for deposits in the Arabian peninsula. Published overdispersion values range from a minimum of approximately 32-35% towards 60-70% or even higher (Armitage *et al.*, 2011; Rosenberg, 2011; Petraglia *et al.*, 2012). There is no clear agreement between authors about which values are most likely to represent well-bleached samples (cf. Groucutt et al., 2015c; Rosenberg, 2011; and Armitage *et al.,* 2011). For these samples, both populations are weakly positively skewed (Figure 5). Interestingly, single grains from ALM3-OSL3 yield both a higher overdispersion value, which corresponds with more scattered data, but the population distribution is more symmetric than that of sample ALM3-OSL2. This sample has been collected from the more heterogeneous, carbonate-rich sediment, therefore we suggest that the increased overdispersion is related to microdosimetric variation in the beta dose (Kalchgruber *et al.*, 2003; Nathan *et al.*, 2003; Guérin *et al.*, 2012). Neither sample's single grain population seems to indicate a problem with either significant partial bleaching (Olley *et al*., 1999; Ballarini *et al*., 2007) or bioturbation (Bateman *et al.*, 2007).

Comparison of multigrain and single grain D_E values highlights a marked discrepancy between these samples. Multigrain and single grain D_Es overlap at one sigma uncertainty for upper sample ALM3-OSL2, however, the multigrain D_E of ALM3-OSL3 is half again as high as its single grain D_E (Figure 5c,d). The relationship between single grain and multigrain measurements is complex, due to the averaging effects of measuring tens or hundreds of grains at the same time in a multigrain aliquot (Arnold and Roberts, 2009) and because of differences in the measurement protocol itself (e.g. relatively constant LED power used for multigrain measurements versus variations in power provided by the single grain laser: Thomsen *et al.*, 2015). In general, however, congruent multigrain and single grain results are believed to show that the D_E obtained is robust, whereas a significant offset may indicate underlying complications such as incomplete signal bleaching (Duller, 2008). We have therefore examined three possibilities that may explain the offset in D_E for sample ALM3-OSL3. These are:

- An unstable medium or slow component in the quartz signal is preferentially measured by the single grain method, leading to an underestimated single grain D_E.
- The characteristics of measured single grains combined when measured via multigrain methods to yield multigrain D_E overestimation.
- Bright, high D_E grains not detected during single grain measurements are causing multigrain D_E overestimation.

We discuss each of these possibilities in detail in Supporting Information Text S1 and Figures S1 to S3, and present further analysis including consideration of both multigrain and single grain D_Es as a function of a modified fast ratio (Madsen *et al*., 2009; Durcan and Duller, 2011; Duller, 2012) and the creation of synthetic aliquots (Henshilwood et al., 2002; Rhodes, 2007) . Based on the evidence presented in the Supporting Information, we suggest that the offset between single and multigrain D_Es for sample ALM3-OSL3 is likely to result from a combination of factors, including the summation of signals from the measured single grain population, as well as the potential presence of bright, high D_E grains not detected by the single grain measurements. Therefore, we calculate ages for this site based on the single grain results, and find that

units 3 and 4 have ages of 56.2 ± 6.5 ka (ALM3-OSL3) and 53.9 ± 4.1 ka (ALM-OSL2) respectively. These ages are stratigraphic order, and suggest that both units were deposited in quick succession.

4.4 Al Marrat 3 lithic assemblage

Excavation at the location of the discrete scatter revealed that the lithics on the slopes of the mesa were eroding from Unit 4. The deepest lithics were securely buried 0.4 m beneath the surface of the IRF. As they were identical in raw material types and technological aspects to those on the slope there was no ambiguity surrounding the fact that they could be classified as the same assemblage. There was no evidence of bioturbation and they derived from highly compacted sediments. The overall assemblage collected (n = 103) is sufficient to provide a technological characterisation. The dominant raw materials were quartz and quartzite, both of which occur locally. A small number (n = 4) of fine-grained igneous artefacts were also identified, from a currently unknown source.

A total of 24 cores were recovered, from both the surface and the excavation (Figure 6, a-d). The core technology is almost exclusively Levallois, with a focus on unidirectional-convergent preparation of the debitage surface often with some supplementary distal/centripetal preparation. Striking platforms are well faceted. With some of the quartz Levallois cores there is often still a considerable amount of cortex at the distal end (Figure 6a). The use of the natural shape to give convexity mirrors arguments about core technology in other contexts (Kuhn, 1995). An additional two cores demonstrate centripetal preparation for a preferential Levallois removal (Figure 6c). The remaining few cores are either at an early stage of reduction or represent simple centripetal flaking in a less organised fashion than with the Levallois cores. The core technology then focused on producing pointed flakes by unidirectional-convergent preparation, along with a less formal core technology to produce small flakes.

Figure 6 - Al Marrat 3 lithics

The flakes can be classified into three groups. Firstly, many are small (~10–40 mm in length) with plain platforms and unidirectional scar patterns, often broken. These appear to be classic core preparation flakes. Secondly, some of the flakes are elongate and are of lateral débordant character (i.e. to exaggerate lateral convexity). Finally, six Levallois flakes are present (Figure 6e-g). These are ~ 60–80 mm in length, with faceted platforms and scar patterns which combine unidirectional-convergent shaping of most of the dorsal surface but with generally short additional removals from distal and the lateral margins. No retouched artefacts were identified.

5. Discussion

Al Marrat 3 provides the first evidence for the incursion of human populations into the arid northern interior of Arabia during early MIS 3. The stratigraphic sequence shows that this occurred in association with the development of a relatively shallow water body within the basin (Figure S4). The sediments of Unit 3 (56.2 ± 6.5 ka, ALM3-OSL3) are indicative of the formation of a low energy, shallow but relatively stable water body or wetland environment. The lithic evidence is found in overlying Unit 4 (53.9 ± 4.1 ka, ALM3-OSL2), which contains evidence for more arid conditions when fluctuations in the depth and salinity of the water body were becoming more strongly seasonal. Grassland vegetation was present with low Panicoid and Chloridoid types present suggesting that C_3 vegetation was the dominant type in the landscape with some mixed C_4 elements. Traces of woody vegetation were present in Unit 5 suggesting a very low background presence of trees or shrubs. Following this period, continuing aridification led to both the desiccation of the sequence, with the exception of phytoliths recorded in Unit 7, and the presumable disappearance of humans from the landscape.

The age of water body formation and the associated human presence at Al Marrat 3 corresponds with an intensification of the monsoon system, as recorded in various marine proxies from the Indian Ocean and Arabian Sea (e.g. Schulz *et al.*, 1998; Altabet *et al.*, 2002; Clemens and Press, 2003;

Higginson *et al.*, 2004; Des Combes *et al.*, 2005; Ivanochko, 2005; Govil and Naidu, 2010; Caley *et al.*, 2011). This period also coincides with a phase of increased westerly-derived rainfall (e.g. Schuldenrein and Clark, 1994; Moumani *et al.*, 2003; Vaks *et al.*, 2006; Cordova *et al.*, 2013). The monsoonal changes are linked to a period of maximum insolation, with a peak at ~ 55 ka. It is unclear, however, which rainfall regime would have been responsible for the increased moisture recorded at Al Marrat 3, since the extent to which monsoon rainfall penetrated into the northern interior ~ 55 ka is uncertain. Evidence for increased humidity in East Africa (Trauth *et al.*, 2003) and in the Sahara (Williams, 2015), and an enhanced flow of the Nile (Revel *et al.*, 2010) suggests increased intensity of the African monsoon during early MIS 3 may have been responsible. A strong N-S precipitation gradient within the Negev suggests that rainfall > 350 mm did not extend southward into Arabia at this time from the Mediterranean (Vaks *et al.*, 2006; 2010), although precipitation insufficient for speleothem growth may have still led to ephemeral drainage activation and wetland development in certain regions. Data from climate models for the period are limited. The HadCM3 model timeslice for 56 ka suggests that the south of Arabia experienced increased precipitation but that the Al Marrat basin remained arid, receiving < 100 mm per year (Figure 7). This model, however, probably underestimates the northward advance of the African monsoon as this was inferred from the comparison of last interglacial models (Jennings *et al.*, 2015). Nonetheless, findings from Al Marrat 3, along with a growing corpus of palaeoenvironmental records from Arabia, now indicate a broad regional hydrodynamic response to increased humidity during early MIS 3, that may have facilitated important demographic shifts.

Figure 7 - A 56 ka timeslice from the HadCM 3 model.

Al Marrat 3 is now one of only three archaeological sites in the entire Arabian Peninsula with assemblages dated to MIS 3 (Figure 1). SD-1 in Yemen (Delagnes *et al.*, 2012) and assemblage A (and possibly B) at Jebel Faya (Armitage *et al.*, 2011) both have different technological characteristics, which may reflect the spatio-temporal complexity of environmental changes at this

time. While the SD-1 and Jebel Faya assemblages are non-Levallois in character, the lithics from Al Marrat 3 demonstrate Levallois reduction methods. It is unclear whether the human group(s) at Al Marrat 3 were Neanderthals or *Homo sapiens*. Neanderthals are known from several sites in the Levant at this time, while if the proposed interpretation of the chronology of the Manot Cave calvaria is accepted then *H. sapiens* may have also been present in SW Asia at ~ 55 ka (Hershkovitz *et al.,* 2015). The Levallois technology recorded at Al Marrat 3 is similar to that of the Levantine Late Middle Palaeolithic, but broadly similar technologies are also found elsewhere, such as in Somalia (Gresham, 1984), and certain MIS 5 contexts associated with *H. sapiens*, e.g. unit XV of Qafzeh Cave (Hovers, 2009). Future comparative studies are therefore required to fully understand the relationship of the Al Marrat 3 lithic assemblage to material from other sites. However, the diversity of lithic assemblages across the peninsula does suggest that complex demographic and cultural change was happening at this time.

6. Conclusion

The site at Al Marrat 3 demonstrates that human populations moved into the interior of the Arabian Peninsula in concert with a short-lived pluvial episode dated to ~ 55 ka. This suggests that even during relatively brief humid periods, human populations were adept at exploiting new habitats, however marginal, deep into the interior of the Arabian Peninsula. The ephemeral nature of the Al Marrat 3 sequence may be attributed to weaker climatic oscillations and lower amounts of precipitation attributed to this pluvial episode, which did not promote the formation of more substantial water bodies, such as those that formed during MIS 5. As such, MIS 3-age records suffer reduced preservation potential and are much more likely to have been affected by erosional processes. Nonetheless, the application of appropriate survey methods as detailed above, has demonstrated the increased potential for identifying further records of this age, raising the possibility of expanding our understanding of human evolution and dispersal in Arabia at this critical time.

Supporting Information

Text S1. Further explanatory information on the offset between single and multigrain D_Es for sample ALM3-OSL3.

Figure S1. Central age model D_E (black circle) and overdispersion (black triangle) values calculated with increasing fast ratio thresholds as a further rejection criterion. Single grain and multigrain data are shown for both ALM3-OSL2 (a,b) and ALM3-OSL3 (c,d).

Figure S2. Synthetic aliquots created for samples ALM3-OSL2 (a,c) and ALM3-OSL3 (b,d). D_E values have been normalized by the single grain CAM D_E for each sample, and the accepted aliquot populations are shown as a historgram (a,b). Accepted aliquot D_E values are also displayed versus the proportion of the net natural signal that can be attributed to the brightest grain in each aliquot (c,d). Data points are classified according to whether that grain was not accepted by the SAR-based rejection criteria, accepted, or accepted but saturated.

Figure S3. Cumulative light sum for all measured quartz grains, excluding those failing the IR depletion ratio (a) and a histogram showing the characteristic D_0 values calculated for accepted grains (b).

Figure S4. Proposed model for the development of palustrine carbonate formation at Al Marrat 3, and the formation of Inverted Relief Features. The human presence coincides with the second half of Phase 4, when climatic conditions become drier and water levels retreated.

Table S1. SAR protocol parameters. A standard Risø TL/OSL TL-DA-15 Mini-sys reader with blue OSL (NSPB-500S LEDs, 470Δ20 nm) and IRSL (Vishay TSFF 5200, 870Δ40 nm nm) stimulation LEDs, $^{90}Sr/^{90}Y$ beta source, and single grain attachment (10 mW, Nd:YVO_4 laser) was used for all

equivalent dose and dose recovery measurements (Bøtter-Jensen et al., 2000; Bøtter-Jensen et al., 2003).

Acknowledgements

We thank His Royal Highness Prince Sultan bin Salman, President of the Saudi Commission for Tourism and Historical Heritage (SCTH), and Prof. Ali Ghabban, Vice President for Antiquities and Museums, for permission to carry out this research. We wish to thank our Saudi colleagues from the SCTH, especially Jamal Omar, Khaled Al Basam, Abdullah Dhawi, Habeeb Turki Abdurahman, Saad Al-Ruwaishan, Althobiti & Sultan Alanzi for their support and assistance with the field investigations. The research was funded by the European Research Council (no. 295719, to MDP).

References

Akazawa T, Aoki K, Bar-Yosef O (eds). 1998. *Neanderthals and Modern Humans in Western Asia*, New York, Plenum Press.

Altabet M, Higginson M, Murray D. 2002. The effect of millennial-scale changes in Arabian Sea denitrification on atmospheric CO_2. *Nature* **415**: 159–162.

Armitage SJ, Jasim SA, Marks AE, Parker AG, Usik VI, Uerpmann HP. 2011. The southern route “Out of Africa”: Evidence for an early expansion of modern humans into Arabia. *Science* **331**: 453–456.

Arnold LJ. Roberts RG. 2009. Stochastic modelling of multi-grain equivalent dose (De) distributions: Implications for OSL dating of sediment mixtures. *Quaternary Geochronology* **4**(3): 204–230.

Ballarini M, Wallinga J, Wintle AG, Bos AJJ. 2007. Analysis of equivalent-dose distributions for single grains of quartz from modern deposits. *Quaternary Geochronology **2*****(**1-4): 77–82.

Bateman MD, Boulter CH, Carr AS, Frederick CD, Peter D, Wilder M. 2007. Detecting post-depositional sediment disturbance in sandy deposits using optical luminescence. *Quaternary Geochronology* ***2***(1-4), 57–64.

Blechschmidt I, Matter A, Preusser F, Rieke-Zapp D. 2009. Monsoon triggered formation of Quaternary alluvial megafans in the interior of Oman. *Geomorphology* **110**: 128–137.

Bøtter-Jensen L, Bulur E, Duller GAT, Murray AS. 2000. Advances in luminescence instrument systems. *Radiation Measurements* **32**: 523–528.

Bøtter-Jensen L., Andersen CE, Duller GAT, Murray AS. 2003. Developments in radiation, stimulation and observation facilities in luminescence measurements. *Radiation Measurements* **37**: 535–541.

Breeze PS, Drake NA, Groucutt HS, Parton A, Jennings RP, White TS, Clark-Balzan L, Shipton C, Scerri EML, Stimpson CM, Crassard R, Hilbert Y, Alsharekh A, Al-Omari A, Petraglia MD. 2015. Remote sensing and GIS techniques for reconstructing Arabian palaeohydrology and identifying archaeological sites. *Quaternary International* **382**: 98-119.

Burns SJ, Fleitmann D, Matter A, Kramers J, Al-Subbary AA. 2003. Indian Ocean Climate and an Absolute Chronology over Dansgaard/Oeschger Events 9 to 13. *Science* **301**(5638): 1365–1367.

Caley T, Malaize B, Zaragossi S, Rossignol L, Bourget J, Eynaud F, Martinez P, Giraudeau J, Charlier K, Ellouz-Zimmermann N. 2011. New Arabian Sea records help decipher orbital timing of Indo-Asian monsoon. *Earth and Planetary Science Letters* **308**(3-4): 433–444.

Clark-Balzan LA, Candy I, Schwenninger J-L, Bouzouggar A, Blockley S, Nathan R, Barton RNE. 2012. Coupled U-series and OSL dating of a Late Pleistocene cave sediment sequence, Morocco, North Africa: significance for constructing palaeolithic chronologies. *Quaternary Geochronology* **12**: 53–64.

Clemens S, Press WL. 2003. A 350,000 year summer-monsoon multi-proxy stack from the Owen Ridge, Northern Arabian Sea. *Marine Geology* **201**: 35–51.

Cordova CE, Nowell A, Bisson M, Ames CJH, Pokines J, Chang M, al-Nahar M. 2013. Interglacial and glacial desert refugia and the Middle Paleolithic of the Azraq Oasis, Jordan. *Quaternary International* **300**: 94–110.

Crassard R, Petraglia MD, Parker AG, Parton A, Roberts RG, Jacobs Z, Alsharekh A, Al-Omari A, Breeze P, Drake NA, Groucutt HS, Jennings RP, Regagnon E, Shipton C. 2013. Beyond the levant:first evidence of a pre-pottery neolithic incursion into the Nefud desert, Saudi Arabia. PLoS One 8, e68061.

Dean WE. 1974. Determination of carbonate and organic matter in calcareous sediments and sedimentary rocks by loss on ignition: Comparison with other methods. *Journal of Sedimentary Pretrology* **44**: 242–248.

Dearing J. 1999. Magnetic susceptibility. In: Walden J, Oldfield F, Smith J (Eds). *Environmental magnetism: A Practical Guide*. Quaternary Research Association Technical Guide 6, Quaternary Research Association, London, 35–63.

Delagnes A, Tribolo C, Bertran P, Brenet M, Crassard R, Jaubert J, Khalidi L, Mercier N, Nomade S, Peigné S, Sitzia S, Tournepiche J.-F, Al-Halibi M, Al-Mosabi A, Macchiarelli R. 2012. Inland human settlement in southern Arabia 55,000 years ago. New evidence from the Wadi Surdud Middle Paleolithic site complex, western Yemen. *Journal of Human Evolution* **63***:* 452–474.

Des Combes HJ, Caulet JP, Tribovillard N. 2005. Monitoring the variations of the Socotra upwelling system during the last 250 kyr: a biogenic and geochemical approach. *Palaeogeography, Palaeoclimatology, Palaeoecology* **223**: 243–259.

Duller G. 2003. Distinguishing quartz and feldspar in single grain luminescence measurements. *Radiation Measurements*, **37**(2): 161–165, 2003.

Duller GAT. 2008. Single-grain optical dating of Quaternary sediments: Why aliquot size matters in luminescence dating. *Boreas*, **37(**4): 589–612.

Duller GAT. 2012. Improving the accuracy and precision of equivalent doses determined using the optically stimulated luminescence signal from single grains of quartz. *Radiation Measurements*, **47(**9): 770–777.

Durcan JA, Duller GAT. 2011. The fast ratio: A rapid measure for testing the dominance of the fast component in the initial OSL signal from quartz. *Radiation Measurements*, **46(**10), 1065–1072.

Eriksson A, Betti L, Friend AD, Lycett SJ, Singarayer JS, Von Cramon N, Valdes PJ, Balloux F, Manica A. 2012. Late Pleistocene climate change and the global expansion of anatomically modern humans. Proceedings of the National Academy of Sciences of the United States of America. **109**(40): 16089–16094.

Farrant AR, Ellison RA, Thomas RJ, Pharaoh TC, Newell AJ, Goodenough KM, Lee JR, Knox RO. 2012. *The geology and geophysics of the United Arab Emirates. Volume 6, Geology of the Western and Central United Arab Emirates*. British Geological Survey, Keyworth, Nottingham.

Faure, G. (1986). *Principles of Isotope Geology*. New York: John Wiley & Sons, Inc.

Fleitmann D, Burns SJ, Pekala M, Mangini A, Al-Subbary A, Al-Aowah M, Kramers J, Matter A. 2011. Holocene and Pleistocene pluvial periods in Yemen, southern Arabia. *Quaternary Science Reviews* **30**: 783–787.

Fu Q. Li H, Moorjani P, Jay F, Slepchenko SM, Bondarev AA, Johnson PL, Aximu-Petri A, Prüfer K, de Filippo C, Meyer M, Zwyns N, Salazar-García DC, Kuzmin YV, Keates SG, Kosintsev PA, Razhev DI, Richards MPP, Peristov

NV, Lachmann M, Douka K, Higham TF, Slatkin M, Hublin JJ, Reich D, Kelso J, Viola TB, Pääbo S. 2014. Genome sequence of a 45,000-year-old modern human from western Siberia. *Nature* **514**: 445–449.

Galbraith, RF, Roberts RG, Laslett GM., Yoshida H, Olley JM. 1999. Optical dating of single and multiple grains of quartz from Jinmium rock shelter, Northern Australia: Part I, Experimental design and statistical models. *Archaeometry* **41**(2): 339–364.

Govil P, Naidu PD. 2010. Evaporation-precipitation changes in the eastern Arabian Sea for the last 68 ka: implications on monsoon variability. *Paleoceanography* **25**, PA1210, doi:10.1029/2008PA001687

Green, RE, Krause J, Briggs AW, Maricic T, Stenzel U, Kircher M, Patterson N, Li H, Zhai W, Hsi-Yang Fritz M, Hansen NF, Durand EY, Malaspinas A-S, Jensen JD, Marques-Bonet T, Alkan C, Prüfer K, Meyer M, Burbano HA, Good JM, Schultz R, Aximu-Petri A, Butthof A, Höber B, Höffner B, Siegemund M, Weihmann A, Nusbaum C, Lander ES, Russ C, Novod N, Affourtit J, Egholm M, Verna C, Rudan P, Brajkovic D, Kucan Z, Gusic I, Doronichev VB, Golovanova LV, Lalueza-Fox C, de la Rasilla M, Fortea J, Rosas A, Schmitz RW, Johnson PLF, Eichler EE, Falush D, Birney E, Mullikin JC, Slatkin M, Nielsen R, Kelso J, Lachmann M, Reich D, Pääbo S. 2010. A draft sequence of the Neanderthal genome. *Science* **328**: 710-722.

Gresham J. 1984. *An investigation of an Upper Pleistocene archaeological site in Northern Somalia*. M.A. Thesis, University of Georgia, Athens.

Groucutt H, Petraglia M, Bailey G, Scerri E, Parton A, Clark-Balzan L, Jennings RP, Lewis L., Blinkhorn J, Drake N, Breeze P, Inglis R, Deves M, Meredith-Williams M, Boivin N, Thomas M, Scally A. 2015a. Rethinking the Dispersal of Homo sapiens out of Africa. *Evolutionary Anthropology* **24**(4): 149–164.

Groucutt HS, Scerri EML, Lewis L, Clark-Balzan L, Blinkhorn J, Jennings RP, Parton A, Petraglia MD. 2015b. Stone tool assemblages and models for the dispersal of Homo sapiens out of Africa, *Quaternary International* **382**: 8–30.

Groucutt HS, White TS, Clark-Balzan L, Parton A, Crassard R, Shipton C, Jennings, RP, Parker AG, Breeze PS, Scerri EML, Abdullah A, Petraglia MD. 2015c. Human occupation of the Arabian Empty Quarter during MIS 5: evidence from Mundafan Al-Buhayrah, Saudi Arabia. *Quaternary Science Reviews* **119**: 116–135.

Groucutt, HS, Shipton C, Alsharekh A, Jennings RP, Scerri, EML, Petraglia MD. 2015d. Late Pleistocene lakeshore settlement in northern Arabia: Middle Palaeolithic technology from Jebel Katefeh, Jubbah. *Quaternary International* **382**: 215–236.

Guérin G, Mercier N, Nathan R, Adamiec G, Lefrais Y. 2012. On the use of the infinite matrix assumption and associated concepts: A critical review. *Radiation Measurements* **47**(9): 778–785.

Heiri O, Lotter AF, Lemcke G. 2001. Loss on ignition as a method for estimating organic and carbonate content in sediments: reproducibility and comparability of results. *Journal of Paleolimnology* **25**: 101–110.

Hemleben C, Meischner D, Zahn R, Almogi-Labin A, Erlenkeuser H, Hiller B. 1996. Three hundred eighty thousand year long stable isotope and faunal records from the Red Sea: Influence of global sea level change on hydrography. *Paleoceanography* **11**(2). 147–156.

Henshilwood CS, D'Errico FD, Yates R, Jacobs Z, Tribolo C, Duller GAT, Wintle AG. 2002. Emergence of Modern Human Behavior: Middle Stone Age Engravings from South Africa. *Science* **295**(5558): 1278–1280.

Hershkovitz I, Marder O, Ayalon A. 2015. Levantine cranium from Manot Cave (Israel) foreshadows the first European modern humans. *Nature* **520**: 216–219.

Higginson M, Altabet MA, Murray DW, Murray RW, Herbert TD. 2004. Geochemical evidence for abrupt changes in relative strength of the Arabian monsoons during a stadial/interstadial climate transition. *Geochimica et Cosmochimica Acta* **68**: 3807-3826.

Hilbert Y, White TS, Parton A. Clark-Balzan L., Crassard R., Groucutt HS, Jennings RP, Breeze P, Parker A, Shipton C, Al-Omari A, Alsharekh A, Petraglia MD. 2014. Epipalaeolithic occupation and paleoenvironments of the Nefud Desert, Saudi Arabia, during the Terminal Pleistocene and Early Holocene. *Journal of Archaeological Science* **50***: 460-74.*

Hijmans RJ, Cameron SE, Parra JL, Jones PG, Jarvis A. 2005. Very high resolution interpolated climate surfaces for global land areas. *International Journal of Climatology* **25**: 1965–1978.

Hoffmann G, Rupprechter M, Rahn M, Preusser F. 2014. Fluvio-lacustrine deposits reveal precipitation pattern in SE Arabia. *Quaternary International* **2015**(382): 145–153.

Hovers E. 2009. *The Lithic Assemblages of Qafzeh Cave*. Oxford University Press, New York.

Ivanochko TS. 2005. Sub-orbital variations in the intensity of the Arabian Sea monsoon. Ph.D. thesis, University of Edinburgh. Available at: http://www.era.lib.ed.ac.uk/handle/1842/760.

Jennings RP, Singarayer J, Stone E., Krebs-Kanzow U, Khon V, Nisancioglu KH, Parker A, Parton A, White TS, Groucutt HS, Petraglia MD. 2015. The greening of Arabia: an ensemble of climate model simulations infers multiple opportunities for human occupation of the Arabian Peninsula during the Late Pleistocene. *Quaternary International* **382**: 181–199.

Kalchgruber R, Fuchs M, Murray AS, Wagner GA. 2003. Evaluating dose-rate distributions in natural sediments using α-Al_2O_3:C grains. *Radiation Measurements* **37**(4-5): 293–297.

Krbetschek MR. 2008. Optically Stimulated Luminescence (OSL) dating of sediments from Jebel al-Emaylah (United Arb Emirates). In: Uerpmann H-P, Jasim SA. (Eds.), The Natural Environment of Jebel al-Buhais: Past and Present. Kerns Verlag, Tübingen, pp. 43–45.

Kuhn S.1995. *Mousterian Lithic Technology: An Ecological Perspective*. Princeton University Press, New York.

Madsen AT, Duller GAT, Donnelly JP, Roberts HM, Wintle AG. 2009. A chronology of hurricane landfalls at Little Sippewissett Marsh, Massachusetts, USA, using optical dating. *Geomorphology*, **109**(1-2): 36–45.

Matter A, Neubert E, Preusser F. 2015 Palaeo-environmental implications derived from lake and sabkha deposits of the southern Rub' al-Khali, Saudi Arabia and Oman. *Quaternary International* **382**: 120–131.

Mellars P, Gori KC, Carr M, Soares PA, Richards MB. 2013. Genetic and archaeological perspectives on the initial modern human colonization of southern Asia. *Proceedings of the National Academy of Sciences* **110**: 10699–10704.

Mclaren, SJ, Al-Juaidi F, Bateman MD, Millington AC. 2008. First evidence for episodic flooding events in the arid interior of central Saudi Arabia over the last 60ka. *Journal of Quaternary Science* **24**: 198–207.

Moumani K, Alexander J, Bateman MD. 2003. Sedimentology of the Late Quaternary Wadi Hasa Marl Formation of Central Jordan: a record of climate variability. *Palaeogeography* **191**:221–242.

Nathan RP, Thomas PJ, Jain M, Murray AS, Rhodes EJ. 2003. Environmental dose rate heterogeneity of beta radiation and its implications for luminescence dating: Monte Carlo modelling and experimental validation. *Radiation Measurements* ***37***(4-5): 305–313.

Olley JM, Murray A, Roberts RG. 1996. The effects of disequilibria in the uranium and thorium decay chains on burial dose rates in fluvial sediments. *Quaternary Science Reviews* **15**: 751–760.

Olley JM, Roberts RG, Murray AS. 1997. Disequilibria in the uranium decay series in sedimentary deposits at Allen's Cave, Nullarbor Plain, Australia: Implications for dose rate determinations. *Radiation Measurements* **27**: 433–443.

Olley JM, Caitcheon GG, Roberts RG. 1999. Origin of dose distributions in fluvial sediments, and the prospect of dating single grains from fluvial deposits using optically stimulated luminescence. *Radiation Measurements*, ***30***(2): 207–217.

Parker AG, Lee-Thorp J, Mitchell P. 2011. Late Holocene neoglacial conditions from the Lesotho highlands, southern Africa: phytolith and stable carbon isotope evidence from the archaeological site of Likoaeng. *Proceedings of the Geologists' Association* **122**: 201–211.

Parton A, Farrant AR, Leng MJ, Schwenninger J-L, Rose JI, Uerpmann H-P, Parker, AG. 2013, An early MIS 3 pluvial phase in Southeast Arabia: Climatic and archaeological implications: *Quaternary International* **300**: 62–74.

Parton A, White TS, Parker AG, Breeze PS, Groucutt HS, Jennings RP, Petraglia, MD. 2015. Orbital-scale monsoon variability and the greening of Arabia as a motor for human dispersal. *Quaternary International.* **382**: 82–97.

Petraglia, MD, Alsharekh AM, Crassard R, Drake NA, Groucutt HS, Parker AG, Roberts RG. 2011. Middle Paleolithic occupation of a Marine Isotope Stage 5 lakeshore in the Nefud Desert, Saudi Arabia. Quaternary Science Reviews **30**: 1555–1559.

Petraglia MD, Alsharekh A, Breeze P, Clarkson C, Crassard R, Drake NA, Groucutt HS, Jennings, RP, Parker AG, Parton A., Roberts RG, Shipton, C. Matheson C., al-Omari A, Veall M-A. 2012. Hominin dispersal into the Nefud

desert and Middle Palaeolithic settlement along the Jubbah palaeolake, northern Arabia. PLoS ONE **11**: e49840.

Revel ME Ducassou FE, Grousset SM, Bernasconi S, Migeon S, Revillon S, Mascle J, Murat A, Zaragosi S, Bosch D. 2010. 100,000 years of African monsoon variability recorded in sediments of the Nile margin, *Quaternary Science Reviews* **29**(11–12): 1342–1362.

Rhodes EJ. 2007. Quartz single grain OSL sensitivity distributions: Implications for multiple grain single aliquot dating. *Geochronometria*, **26**:19–29.

Rosenberg TM, Preusser F, Fleitmann D, Schwalb A, Penkman K, Schmid TW, Al-Shanti MA, Kadi K, Matter A. 2011. Late Pleistocene pluvial periods in southern Arabia - windows of opportunity for modern human dispersal. *Geology* **39**: 1115–1118.

Rosenberg TM, Preusser F, Risberg J, Plikk A, Kadi KA, Matter A. Fleitmann D. 2013. Middle and Late Pleistocene humid periods recorded in palaeolake deposits of the Nafud desert, Saudi Arabia. *Quaternary Science Reviews*, **70**: 109–123.

Schuldenrein J, Clark GA. 1994. Landscape and prehistoric chronology of west–central Jordan. *Geoarchaeology*, **9**(1): 31–55.

Schulz H., von Rad U. Erlenkeusser H. 1998. Correlations between Arabian Sea and Greenland climate oscillations of the past 110,000 years. *Nature*, **393**: 54–57.

Scerri EML, Breeze P, Parton A, Groucutt HS, Stimpson C, White T, Stimpson C, Clark-Balzan L, Jennings RP, Alsharekh A, Petraglia MD. 2015. Middle to Late Pleistocene human habitation in the western Nefud Desert, Saudi Arabia. *Quaternary International*. **382**: 200–214.

Shea J. 2003. Neandertals, competition, and the origin of modern human behavior in the Levant. *Evolutionary Anthropology* **12**:173–187.

Thomsen KJ, Kook M, Murray AS, Jain M, Lapp T. 2015. Single-grain results from an EMCCD-based imaging system. *Radiation Measurements* **81:**185–191.

Trauth MH, Maslin MA, Deino AL, Strecker MR, Bergner AGN, Duhnforth M. 2007. High- and low-latitude forcing of Plio-Pleistocene East African climate and human evolution. *Journal of Human Evolution* **53**: 475–486.

Vaks A, Bar-Matthews M, Ayalon A, Frumkin A, Dayan U, Halicz L, Almogi-Labin A, Schilman B. 2006. Paleoclimate and location of the border between Mediterranean climate region and the Saharo–Arabian Desert as revealed by speleothems from the northern Negev Desert, Israel. *Earth and Planetary Science Letters* **249**: 384–399.

Vaks A, Bar-Matthews M, Matthews A, Ayalon A, Frumkin A. 2010. Middle-Late Quaternary paleoclimate of northern margins of the Saharan-Arabian Desert: reconstruction from speleothems of Negev Desert, Israel. *Quaternary Science Reviews* **29**: 2647–2662.

Williams M, Duller G, Williams F, Woodward J, Macklin MG. 2015. Causal links between Nile floods and eastern Mediterranean sapropel formation during the past 125 kyr confirmed by OSL and radiocarbon dating of Blue and White Nile sediments. *Quaternary Science Reviews* **130**: 89-108

Figures

Figure 1: Location of Al Marrat basin and archaeological sites mentioned in the text.

Figure 2: The Al Marrat basin, remotely sensed data and the distribution of archaeological sites recorded on the basin survey. The sites included Lower and Middle Palaeolithic stone tool scatters, and late prehistoric rock art and megalithic structures. Clockwise from top; Shaded relief map of the Al Marrat Basin and surroundings, showing modelled lake extents (blue), archaeological sites of the ALM basin (numbered), detected (red) palaeolake deposits and

additional areas of indurated calcretized deposits (grey) as underlay. Photograph of identified gypsiferous IRFs in the field (fore and midground raised pale deposits). Landsat Thermal Mapper RGB (7,4,1) false colour composite (FCC) showing automatically mapped IRFs (outlined in red), and additional area of heavily indurated calcrete (grey outline) in FCC data.

Figure 3: Plan view of the Inverted Relief Feature at Al Marrat 3, which is visible in the inset photograph, and the location of the excavation trench and surface lithic scatter. Lithics in red are derived from within Unit 4 at a depth of 0.40 m below the surface.

Figure 4: Stratigraphy and multiproxy data from Al Marrat 3, showing fine fraction (<2 mm) granulometry, magnetic susceptibility values, and organic and carbonate content. See text for details.

Figure 5 : Luminescence characteristics and accepted D_E populations. Natural decay curves (inset) and growth curves shown for an accepted single grain (a) and an accepted multigrain aliquot (b) from sample ALM3-OSL3. Accepted single grain D_Es (filled black circles) and multigrain D_Es (white diamonds) calculated for ALM3-OSL2 (c) and ALM3-OSL3 (d).

Figure 6: Selection of the lithic assemblage from Al Marrat 3. Photo H. Groucutt. Lithics made on quartz (A, B) and quartzite (C-G). Cores (A-D), unidirectional-convergent Levallois cores (A, B, D) and preferential Levallois core with centripetal preparation (C.). Levallois flakes (E-G), with faceted striking platforms and unidirectional-convergent scar patterns supplemented by removals from the laterals and distal.

Figure 7: HadCM3 climate model of the Arabian Peninsula at 56 ka (modified from Jennings *et al.* (2015). Based on the results from Al Marrat 3, the model would appear to underestimate the northern spatial distribution of summer rainfall from North Africa at this time.

Tables

Table 1. Numbers of OSL aliquots/grains excluded according to each rejection criterion (see key below), with central age model equivalent doses and overdispersion values calculated for accepted populations. Measurement type (i.e. dose recovery experiment or D_E measurements intended for age calculations) and scale of analysis (multigrain, 'MG', or single grain, 'SG') are indicated for each data set.

			Number Rejected								
Sample	Meas. Type	Meas. (#)	<3σ	T_N Err.	RR	Zero	IR	Sat.	Accepted	CAM D_E (Gy)	Overdispersion (%)
ALM3-OSL2	Age (MG)	18	0	0	2	0	1	0	15	80.9 ± 6.3	29.3 ± 5.7
	Age (SG)	2100	1699	342	14	2	7	2	34	72.6 ± 4.8	30.7 ± 5.6
ALM3-OSL3	Dose Recovery (MG)	6	0	0	0	0	1	0	5	1.01 ± 0.04*	N.A.
	Age (MG)	18	0	0	2	0	1	1	14	147.0 ± 15.3	38.0 ± 7.6
	Age (SG)	1100	892	162	10	0	3	5	28	90.0 ± 9.2	45.7 ± 8.1

*Common age model used due to lack of overdispersion. The D_E reported here is the recovered dose normalized by the given dose (136.6 ± 2.7 Gy).

Aliquots were rejected if they did not meet the following criteria:

'<3σ': The net natural test dose signal is greater than three times the standard deviation of the background.

'T_N Err.': The natural test dose error is less than 20% of the test dose response.

'RR': The ratio of the repeated dose step to the first given dose ('recycling ratio') is within 10% of unity, or the recycling ratio was consistent with unity at 2 sigma.

'Zero': The ratio of the normalized OSL response of the zero dose step to the natural signal ('zero ratio') isless than 5%, or the zero ratio was consistent with 0 at 2 sigma.

'IR': The ratio of the post-IR repeated dose step to the first given dose ('IR depletion ratio') is greater than 0.9, or the IR depletion ratio was consistent with unity at 2 sigma.

'Sat': Aliquots were considered to be saturated if the natural response plus error is greater than the fitted exponential (i.e. Analyst returns an infinite error), or the normalized natural signal (L_n/T_n) never intersects with the dose response curve.

Table 2: Values for dose rate calculations and final ages. The cosmic dose rate was calculated with current burial depth and an average overburden density of 1.9 g cm^{-3}. An average water content of 5 ± 3% (mass of water in wet sediment) was assumed for both samples; this value was used to correct the dry gamma dose rates measured on site with a gamma spectrometer.

Sample	K (%)	Th (ppm)	U (ppm)	Dry Gamma Dose Rate (Gy ka^{-1})	Burial Depth (m)	Total Wet Dose Rate (Gy ka^{-1})	Age (ka) Single Grain	Age (ka) Multi-grain
ALM3-OSL2	0.35	1.50	2.80	0.57 ± 0.03	0.52	1.35 ± 0.05	53.9 ± 4.1	60.1 ± 5.2
ALM3-OSL3	0.37	1.60	3.00	0.85 ± 0.04	0.82	1.60 ± 0.09	56.2 ± 6.5	91.7 ± 10.8

Table 3: Archaeological sites found within the Al Marrat basin

Site code	Type	Period	Lat	Long	Description
ALM 1	Lithics	Middle Palaeolithic	27°44 '22"	40°30 '31"	Low density lithic scatter
ALM 2	Cairns	Unknown: Often date to the Chalcolithic and Bronze Age	27°43 '25"	40°28 '33"	Scattered burial cairns on the talus slopes of the jebel to the west of the basin
ALM 3	Lithics	Middle Palaeolithic	27°43 '58"	40°29 '5"	High density of Middle Palaeolithic stone stools, some securely stratified within a mesa
ALM 4	Rock art	Early Holocene and Iron Age	-	-	Multiple rock art panels on the southern jebel lower slopes. Includes depictions of cattle and ibex
ALM 5	Lithics	Middle Palaeolithic	27°19 '23"	40°28 '57"	Lithics deposited on heavily indurated calcretes
ALM 6	Lithics	Lower Palaeolithic	27°43 '36"	40°28 '56"	Lithics deposited on heavily indurated calcretes
ALM 7	Lithics	Lower Palaeolithic	27°43 '38"	40°28 '59"	Lithics deposited on heavily indurated calcretes

Table 4: Phytoliths counts from the stratigraphic sequence at Al Marrat 3. Note that dashes represent values too low to calculate percentage values. The phytoliths were recovered from environmental samples taken securely within each unit at different positions along the west-facing section of the excavation trench shown on Figure 3. Note that sample # 1 derived from a pocket of Unit 7 material within Unit 6, hence its depth overlapping with that of sample # 2.

Sample number	Depth range	Unit	Round	%	Oblong	%	Square/Rectangle	%	Round-Trapezoid	%	Rondel	%	Bilobate	%	Polylobate	%	Crossbody	%	Saddle	%	Flat Tower	%
1	19/5	7	68	21.1	83	25.7	81	25.1	0	0.0	9	2.8	4	1.2	1	0.3	0	0.0	12	3.7	0	0.0
2	27/10	6	1	-	2	-	8	-	0	-	1	-	1	-	0	-	0	-	2	-	0	-
3	34/25	5	41	22.7	49	27.1	38	21.0	1	0.6	7	3.9	2	1.1	0	0.0	0	0.0	2	1.1	0	0.0
4	40/45	4	55	31.3	35	19.9	30	17.0	5	2.8	4	2.3	2	1.1	0	0.0	0	0.0	3	1.7	1	0.6
5	51/35	4	5	-	1	-	1	-	0	-	0	-	0	-	0	-	0	-	0	-	1	-
6	65/70	3	15	23.4	24	37.5	10	15.6	1	1.6	1	1.6	2	3.1	0	0.0	2	3.1	0	0.0	0	0.0
7	109/88	2	1	-	1	-	0	-	0	-	0	-	0	-	0	-	0	-	0	-	0	-

Sample number	Depth range	Unit	Angle	%	Circular rugose	%	Corklike	%	trapezoid	%	elongated/dendriform	%	point shaped	%	bulliform	%	stomata	%	Short cells	%	Long cells	%	Total (n)
1	19/5	7	10	3.1	4	1.2	1	0.3	0	0.0	25	7.7	19	5.9	4	1.2	2	0.6	273	84.5	50	15.5	323
2	27/10	6	2	-	0	-	0	-	0	-	0	-	0	-	0	-	0	-	17	-	0	-	17
3	34/25	5	6	3.3	2	1.1	0	0.0	1	0.6	15	8.3	11	6.1	4	2.2	2	1.1	149	82.3	32	17.7	181
4	40/45	4	6	3.4	0	0.0	1	0.6	0	0.0	6	3.4	8	4.5	20	11.4	0	0.0	142	80.7	34	19.3	176
5	51/35	4	0	-	0	-	0	-	1	-	1	-	3	-	2	-	1	-	9	-	7	-	16
6	65/70	3	1	1.6	0	0.0	0	0.0	1	1.6	3	4.7	1	1.6	3	4.7	0	0.0	57	89.1	7	10.9	64
7	109/88	2	1	-	0	-	0	-	0	-	1	-	0	-	0	-	0	-	3	-	1	-	4

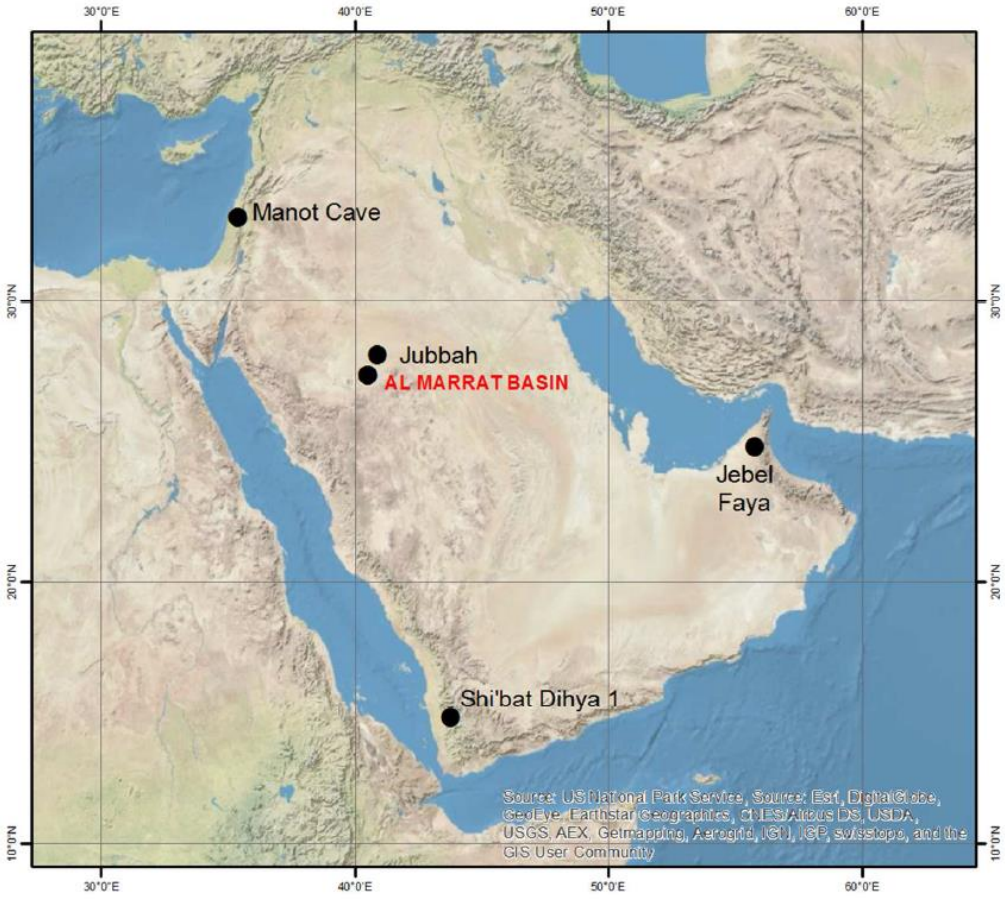

Figure 1: Location of Al Marrat basin and archaeological sites mentioned in the text.

.

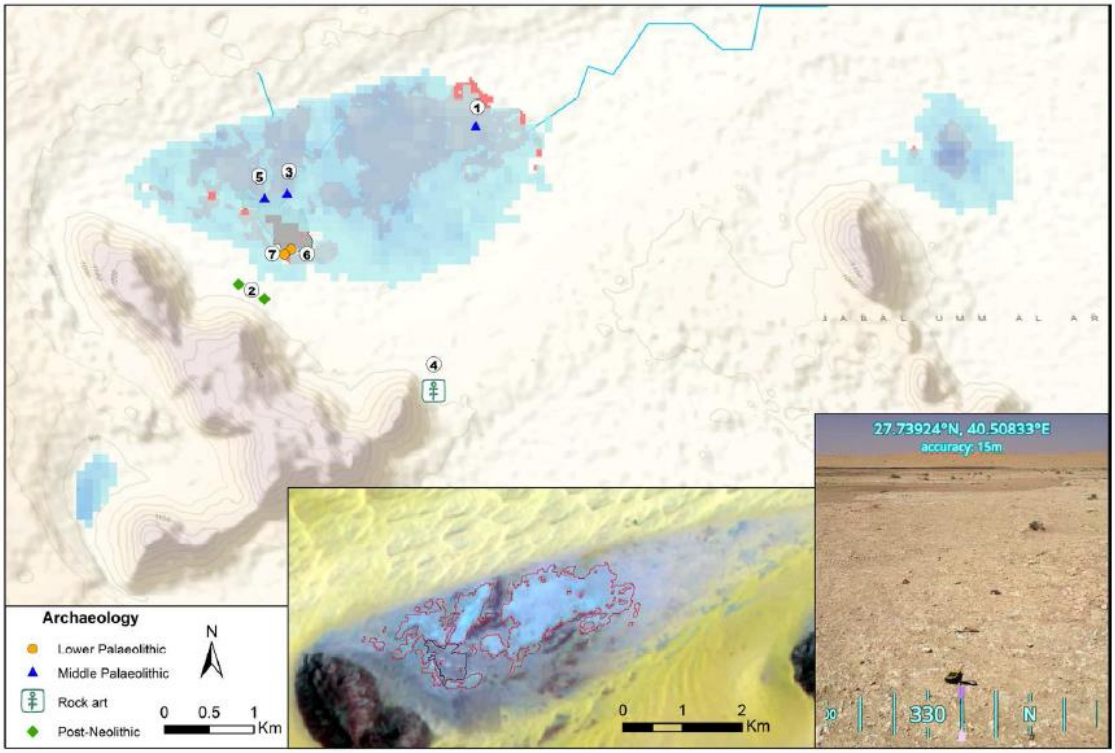

Figure 2: The Al Marrat basin, remotely sensed data and the distribution of archaeological sites recorded on the basin survey. The sites included Lower and Middle Palaeolithic stone tool scatters, and late prehistoric rock art and megalithic structures. Clockwise from top; Shaded relief map of the Al Marrat Basin and surroundings, showing modelled lake extents (blue), archaeological sites of the ALM basin (numbered), detected (red) palaeolake deposits and additional areas of indurated calcretized deposits (grey) as underlay. Photograph of identified gypsiferous IRFs in the field (fore and midground raised pale deposits). Landsat Thermal Mapper RGB (7,4,1) false colour composite (FCC) showing automatically mapped IRFs (outlined in red), and additional area of heavily indurated calcrete (grey outline) in FCC data.

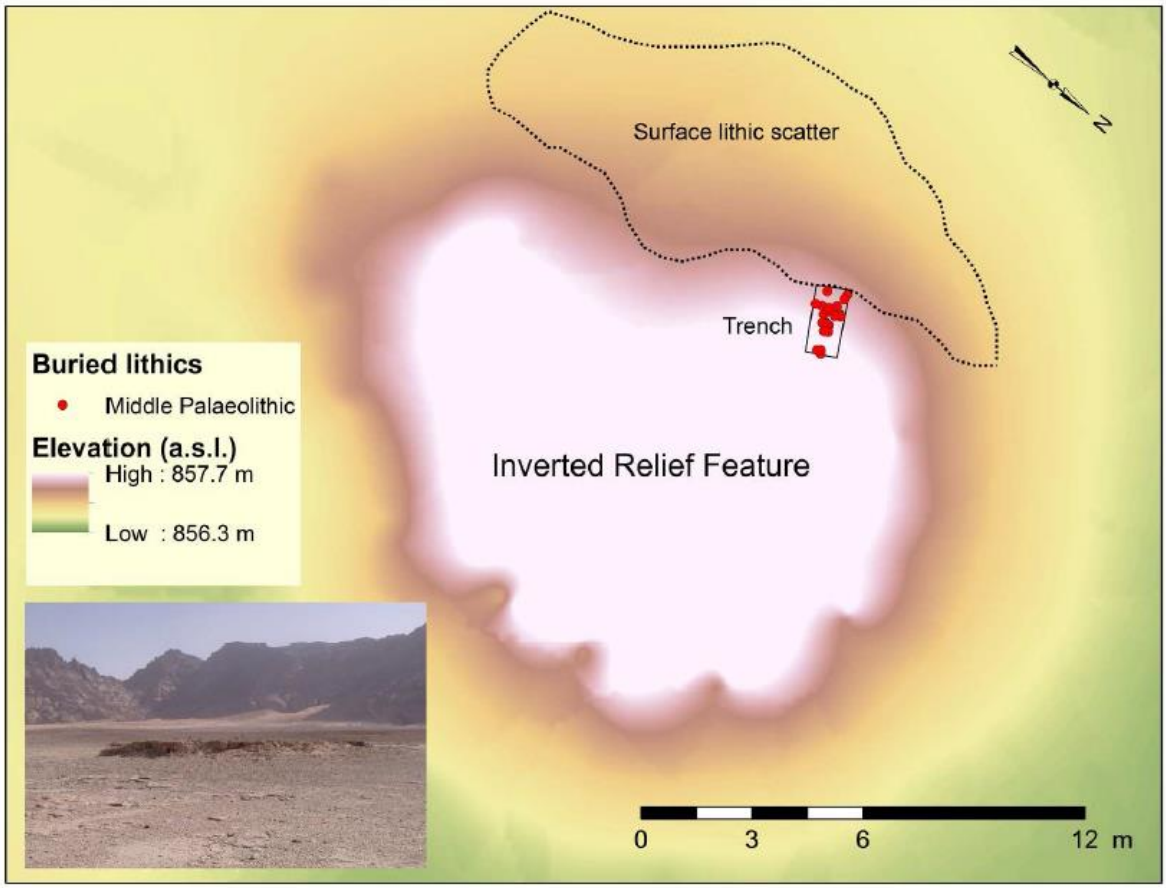

Figure 3: Plan view of the Inverted Relief Feature at Al Marrat 3, which is visible in the inset photograph, and the location of the excavation trench and surface lithic scatter. Lithics in red are derived from within Unit 4 at a depth of 0.40 m below the surface

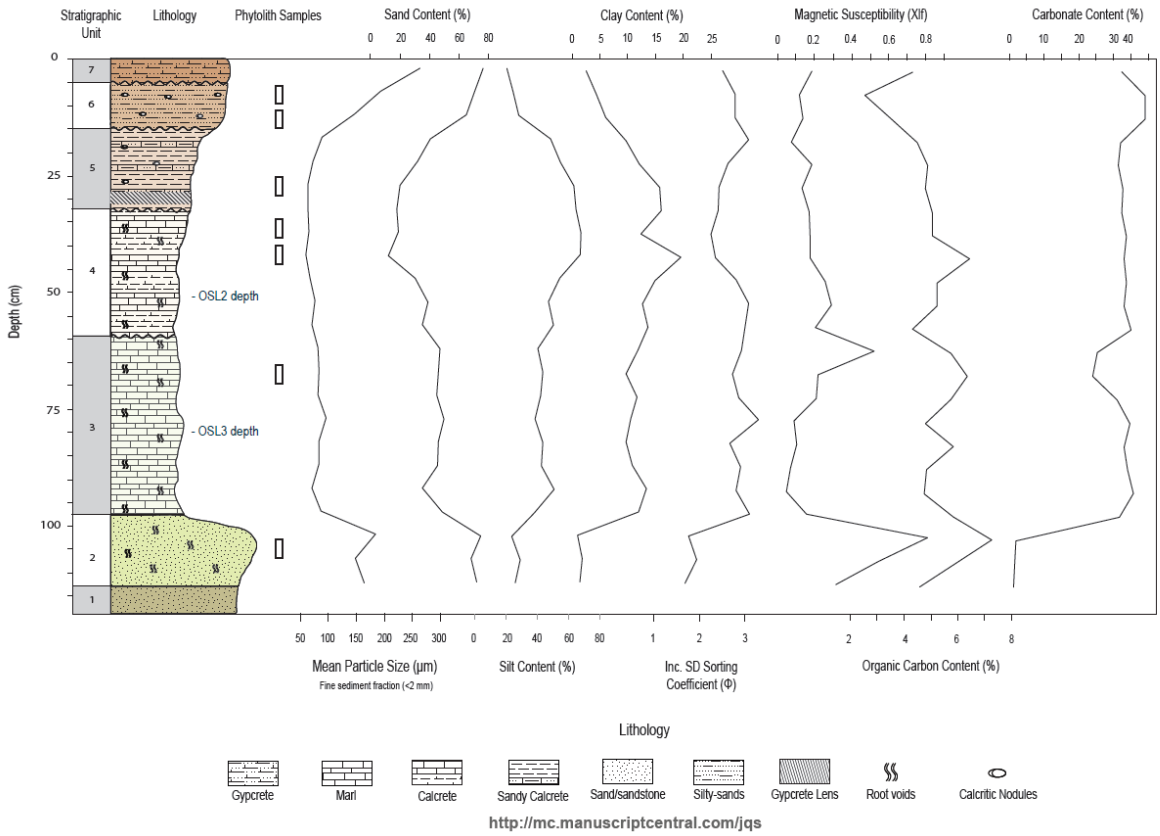

Figure 4: Stratigraphy and multiproxy data from Al Marrat 3, showing fine fraction (<2 mm) granulometry, magnetic susceptibility values, and organic and carbonate content. See text for details.

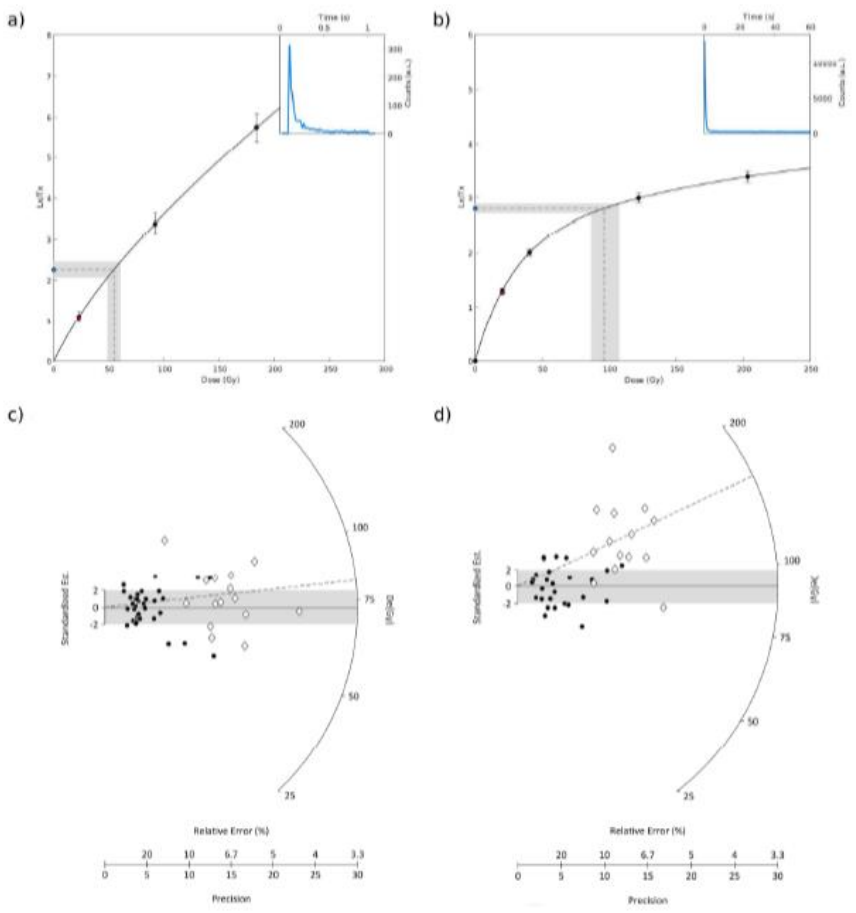

Figure 5 : Luminescence characteristics and accepted D_E populations. Natural decay curves (inset) and growth curves shown for an accepted single grain (a) and an accepted multigrain aliquot (b) from sample ALM3-OSL3. Accepted single grain D_Es (filled black circles) and multigrain D_Es (white diamonds) calculated for ALM3-OSL2 (c) and ALM3-OSL3 (d).

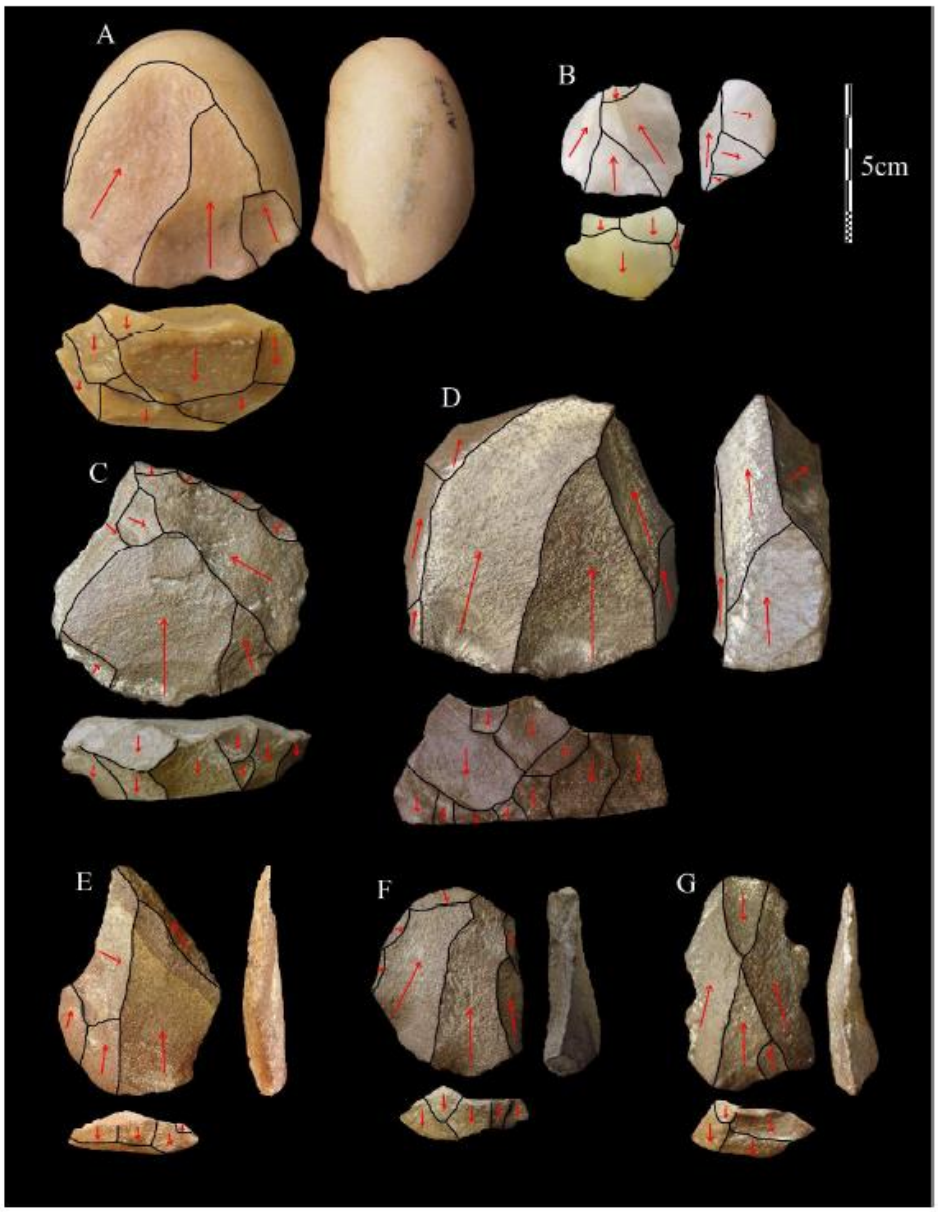

Figure 6: Selection of the lithic assemblage from Al Marrat 3. Photo H. Groucutt. Lithics made on quartz (A, B) and quartzite (C-G). Cores (A-D), unidirectional-convergent Levallois cores (A, B, D) and preferential Levallois core with centripetal preparation (C.). Levallois flakes (E-G), with faceted striking platforms and unidirectional-convergent scar patterns supplemented by removals from the laterals and distal.

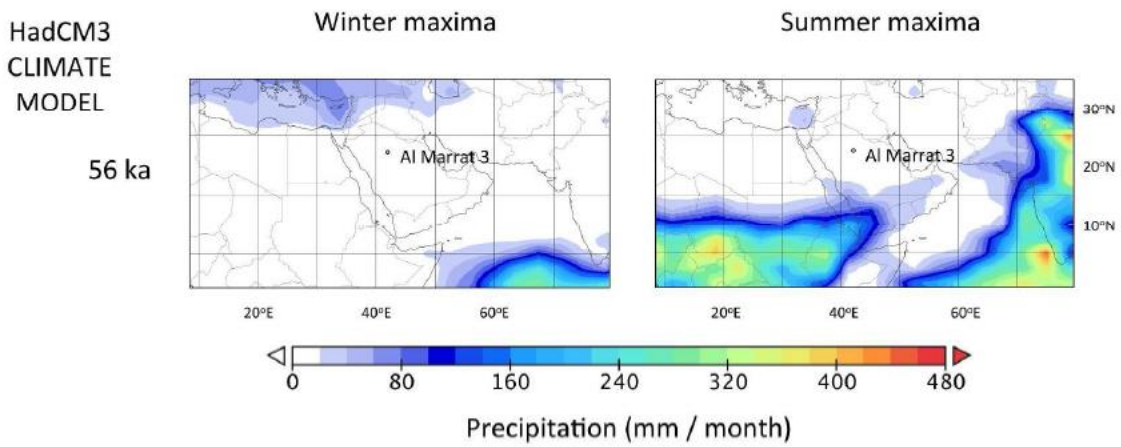

Figure 7: HadCM3 climate model of the Arabian Peninsula at 56 ka (modified from Jennings *et al.* (2015). Based on the results from Al Marrat 3, the model would appear to underestimate the northern spatial distribution of summer rainfall from North Africa at this time.